Further investigation on water-hammer control inline strategy in water-supply systems

Ali Triki

ABSTRACT

This paper revisited the inline re-design strategy used for water-hammer control into an existing steel-piping water supply system to further promote a comprehensive exploration of the entire design driven parameters set, including pressure-head, circumferential-stress and radial-strain behaviors. This strategy consists of replacing a short-section of the transient sensitive region of the original piping system by another made of polymeric pipe-wall material. The 1-D unconventional water-hammer model embedding the Vitkovsky and the Kelvin–Voigt formulations was adopted to describe the flow behavior and solved by the Method of Characteristics (MOC). The model was used to investigate two critical scenarios, including water-hammer up- and down-surge events. The effectiveness of the proposed strategy was evaluated for the high- or low-density polyethylene (HDPE or LDPE) material used for the replaced short-section pipe-wall. Results suggested that the utilized strategy could be successfully employed to amortize pressure-head and circumferential-stress rise and drop. Moreover, the observed amortization rates were found to be strongly dependent upon the short-section material and size. However, two interesting characteristics of the control strategy at hand, not previously reported, also emerged from this study, including the amplification of the radial-strain peaks (and ridges) along with the spread-out of the wave oscillation period.

Key words | column-separation, Kelvin-Voigt formulation, LDPE/HDPE pipe-wall material, method of characteristics, Vitkovsky formulation, water-hammer control

Ali Triki
Research Unit: Mechanics, Modelling Energy and Materials M2EM,
National Engineering School of Gabes,
University of Gabes,
Zrig 6029,
Tunisia
E-mail: *ali.triki@enis.rnu.tn*

INTRODUCTION

The incidence of water-hammer surges can potentially have adverse impacts on the performance of water supply infrastructures and the safety of users and operators. These surges are closely associated with flow disturbances due to either normal operations or accidental events, such as pump shutdowns/starts or rapid changes in control valve settings. These events trigger a series of water-hammer up- and down-surges (also referred to as positive- and negative-surges), which may cause serious perturbation in the serviceability of water supply systems as well as risks to operators' safety. Bergant *et al.* (2006) conducted an exhaustive review and evaluated a wide range of water-hammer severe consequences which include mainly disruption of normal control operations, excessive noise, fatigue and stretch of the pipe-wall. In more dramatic situations, these surges may lead to pipe rupture, separation at bends and damage to other devices forming part of the hydraulic system. Besides, potential failure mechanisms arise from the liquid column separation onset, also known as cavitation. This situation occurs whenever the local static pressure of the fluid falls below its saturated pressure value, during water-hammer courses, which causes the liquid column to separate, and subsequently, after cavity collapse, the flow behavior results in short duration pressure pulses superimposed on water-hammer waves. Such a circumstance may dramatically bring about the pipe collapse, the complete failure of the hydraulic system, and even dangerously affect the operator's safety (Bergant *et al.* 2006).

doi: 10.2166/aqua.2017.073

Obviously, these surges cannot be avoided completely. Nonetheless, several design measure proposals are available to minimize their severe impact to a desirable extent, while providing an adequate service level (pressure and flow capacities). In essence, the conventional utilized strategies include three main modules: (1) alteration of pipeline properties (Boulos *et al.* 2005a, 2005b); (2) implementation of operational control strategies (Seog & Karney 2004); and (3) installation of additional surge control devices (Pejovic *et al.* 1987; Boulos *et al.* 2005a). Generally, a combination of multiple devices is used in practice. However, this method may negatively affect the performance of the hydraulic system due to the cumulative use of control devices (Pothof & Karney 2012).

Alternatively, recent researches on pipe-wall materials have highlighted the ability of highly deformable pipe-wall materials, such as high- or low-density polyethylene (HDPE or LDPE), to significantly soften transient pressure fluctuations during high- and low-pressure surge loading (Güney 1983; Brinson & Brinson 2008). Indeed, the viscoelastic behavior of polymeric material is characterized by a time dependent material response (i.e. retarded response) between the pressure rise (or drop) and the pipe-wall expansion (or contraction), besides the elastic response observed in the case of rigid pipe-wall material (Covas *et al.* 2004, 2005; Soares *et al.* 2008, 2012; Evangelista *et al.* 2015).

In this context, a significant investigation was previously launched by Massouh & Comolet (1984). Specifically, the authors addressed experimental observations relating to the efficiency of adding a short rubber-pipe in-series to a main steel-piping system to dampen water-hammer upsurge waves. The authors observed a significant damping of pressure rise accompanied with gradually varied oscillations and a relatively long period of pressure wave oscillations.

From a design point of view, an efficient numerical model is certainly a valuable tool to accurately predict and analyze the hydraulic transient behavior under a set of real or hypothetical conditions.

Classically, safety criteria include a minimum pipe size, extreme pressure-head values, maximum allowable flowrate and the duration of water-hammer event. However, other fundamental design parameters, often neglected in the design stage, including the circumferential-stress and the radial-strain behaviors, should also be considered. Specifically, the two latter parameters are mainly embedded in the fatigue damage of hydraulic machineries or system parts.

Previous results on the inline strategy used for water-hammer control into steel-piping system were investigated by the author (Triki 2016), using the Ramos *et al.* (2004) model. This strategy was based on replacing a short-section of the main existing pipe by another made of (HDPE or LDPE) polymeric material. Specifically, results confirmed that such a strategy could significantly reduce both up- and down-surge pressure heads. Nonetheless, apart from acknowledgment of pressure-head evolutions, there was no established calculation regarding the circumferential-stress and the radial-strain behaviors in previous investigations. Insofar as the latter two parameters are equally embedded in the design stage, a call for a better predictive model providing relevant information to the designer needs to be carefully selected. Alternatively, the Vitkovsky *et al.* (2000) unsteady friction and the Kelvin–Voigt pipe-wall behavior formulations (Covas *et al.* 2004, 2005; Triki 2017) might be successfully used, in conjunction with the classical water-hammer models, in order to deliver more desirable design estimates of supplement parameters such as the circumferential-stress and the radial-strain evolutions throughout the piping system, besides the pressure-head behavior. Furthermore, such an unconventional water-hammer model was recognized to have the desirable accuracy attribute in reproducing experimental data (Covas *et al.* 2004).

Thereby, to address these limitations, we planned in this paper to revisit the efficiency of the inline design strategy by addressing a comprehensive evaluation of the full design parameter set, including pressure-head, circumferential-stress and the radial-strain, during the hydraulic transient process. Accordingly, the unconventional water-hammer model based on the Vitkovsky and the Kelvin–Voigt formulations can be made suitable for this study insofar as the outcome of this model provides information about the entire set of the required design parameters.

METHODS

As per Covas *et al.* (2004), the 1-D unconventional water-hammer model based on the Vitkovsky and the

Kelvin–Voigt formulations can be written as follows:

$$\begin{cases} \dfrac{\partial H}{\partial t}+\dfrac{a_0^2}{gA}\dfrac{\partial Q}{\partial x}+2\dfrac{a_0^2}{g}\dfrac{d\varepsilon_r}{dt}=0 \\ \dfrac{1}{A}\dfrac{\partial Q}{\partial t}+g\dfrac{\partial H}{\partial x}+g(h_{f_s}+h_{f_u})=0 \end{cases} \tag{1}$$

Here, H and Q represent the pressure-head and the flow rate; A designates the cross-sectional area of the pipe; g denotes the gravity acceleration; $a_0=\sqrt{(K/\rho)/\{1+\alpha'(D/e)KJ_0\}}$ is the elastic-wave speed; J_0 is the elastic creep-compliance; α' is the pipe-wall constraint coefficient ($\alpha'=1$, for thin wall elastic pipes (Wylie & Streeter 1993; Ghidaoui *et al.* 2005; Kaveh *et al.* 2010)); D and e are the pipe inner diameter and the pipe-wall thickness, respectively; and x and t denote the axial coordinate and time, respectively.

The quasi-steady friction losses component per unit length h_{f_s} is computed for turbulent and laminar flow, respectively, as follows:

$$h_{f_s}=RQ|Q| \quad \text{and} \quad h_{f_s}=\frac{32\nu'}{gD^2A}|Q| \tag{2}$$

where $R=f/2gDA^2$ corresponds to the pipe resistance; ν' and f refer to the kinematic fluid viscosity and the Darcy–Weisbach friction factor, respectively.

The unsteady friction losses component h_{f_u} evaluated according to Vitkovsky *et al.* (2000), yields:

$$h_{f_u}=\frac{k_v}{gA}\left(\frac{\partial Q}{\partial t}+a_0\,Sgn(Q)\left|\frac{\partial Q}{\partial x}\right|\right) \tag{3}$$

in which k_v is the Vitkovsky *et al.* (2000) decay coefficient.

The retarded component of the radial-strain ε_r, evaluated referring to 'Boltzmann superposition principle' schematically shown in Figure 1 (i.e. a combination of stresses that acts independently results in strains that can be added linearly (Aklonis *et al.* 1972)), yields:

$$\varepsilon_r(t)=\int_0^t \sigma(t-t')\left(\frac{\partial J(t')}{\partial t'}\right)dt' \tag{4}$$

where $\sigma=\alpha'\Delta pD/2e$ is the total circumferential-stress and $J(t)$ is the creep-compliance function describing the rheological behavior of the pipe-wall, which may be calculated using the generalized Kelvin–Voigt linear-viscoelastic mechanical model schematized in Figure 2 as follows (Aklonis *et al.* 1972):

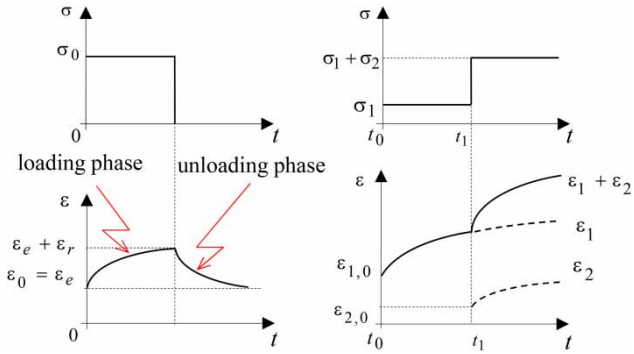

Figure 1 | Schematic diagram of stress and strain evolutions due to an instantaneous pressure load/unload, according to the 'Boltzmann superposition principle'.

$$J(t)=J_0+\sum_{k=1}^{n_{kv}}J_k\left(1-e^{-t/\tau_k}\right) \tag{5}$$

where $J_0=1/E_0$ is the creep compliance of the first spring, E_0 is the dynamic modulus of elasticity of the pipe wall; for each kth Kelvin–Voigt element, $J_k=1/E_k$ and $\tau_k=\mu_k/E_k$ ($k=0\cdots n_{kv}$) are the spring creep compliance coefficient and the retardation time of the dashpot, respectively; E_k and μ_k ($k=1\cdots n_{kv}$) are the modulus of elasticity of the spring and the viscosity of the dashpot, respectively, where n_{kv} is the number of Kelvin–Voigt elements.

The numerical analysis step, involving the unconventional water-hammer solution, is presented in the next section.

Fixed-grid method of characteristics with specified time interval (FG-MOC)

Conventionally, the numerical solution of the unconventional water-hammer Equations (1) and (2) is derived using the FG-MOC for handling the flow problems investigated thereafter,

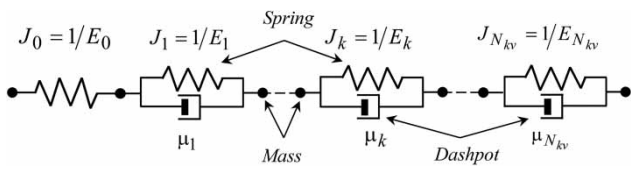

Figure 2 | Schematic illustration of the generalized Kelvin–Voigt linear viscoelastic mechanical model (with N_{kv} elements).

involved with the series connection of multiple pipes (with variable wave speeds). Accordingly, the corresponding compatibility equations solved by the finite difference scheme along the set of characteristic lines yield (Ghidaoui & Karney 1994; Soares *et al.* 2008; Niroomandi *et al.* 2012):

$$\mathbf{C}^{j\pm}: \frac{dH}{dt} \pm \frac{a_0^j}{gA^j}\frac{dQ}{dt} + \frac{2a_0^2}{g}\left(\frac{\partial \varepsilon_r}{dt}\right) \pm a_0^j h_f^j = 0 \text{ along } \frac{\Delta x^j}{\Delta t} = \pm \frac{a_0^j}{C_r^j} \tag{6}$$

in which, C_r^j is the Courant number specified in the range $0 \prec C_r \leq 1$, being used to allow the grid points to coincide with the intersection of the characteristic curves; the superscript j indicates the pipe number ($1 \leq j \leq np$) and the lower subscript i indicates the section number of the jth pipe ($1 \leq i \leq n_s^j$); n_s^j denotes the number of sections of the jth pipe and np denotes the number of pipes; Δt and Δx designate the time- and space-step increments, respectively.

From a practical stand point, the time step is selected from the shortest pipe and the Courant number is set to unity ($C_r^j = 1$). Secondly, the space-step increment is selected for the remaining pipes using the Courant–Frederic–Lewy condition: $C_r^j = a_0^j \Delta t / \Delta x^j \leq 1$ (Wylie & Streeter 1993).

Hence, the numerical solution at any time step, determined directly from Equation (6), yields (Soares *et al.* 2008):

$$\mathbf{C}^{\pm}: \begin{cases} Q_{i,t}^j = c_p^j - c_a^j H_{i,t}^j \\ Q_{i,t}^j = c_n^j + c_a^j H_{i,t}^j \end{cases} \text{ along } \frac{\Delta x^j}{\Delta t} = \pm \frac{a_0^j}{C_r^j} \tag{7}$$

where $c_p^j = (Q_{i-1,t-1}^j + (1/B^j) H_{i-1,t-\Delta t}^j + c_{p1}''^j + c_{p1}'''^j)/(1 + c_p'^j + c_{p2}''^j + c_{p2}'''^j)$; $c_n^j = (Q_{i+1,t-1}^j + (1/B^j) H_{i+1,t-\Delta t}^j + c_{n1}'' + c_{n1}''')/(1 + c_n'^j + c_{n2}''^j)$; $c_{a+}^j = 1 + c_{p2}'''^j/(B^j(1 + c_{p2}'^j + c_{p2}''^j))$; the series sets of coefficients: $\{C_p'^j; C_n'^j\}$; $\{C_{p1,2}''^j; C_{n1,2}''\}$, and $\{C_{p1,2}'''^j; C_{n1,2}'''\}$, related to the discretization of steady friction, unsteady friction and the linear viscoelastic rheological behavior of pipe-wall terms, respectively, are listed in Table 1.

Table 1 | Constant coefficients of Equation (7) $\{c_p^j; c_n^j; c_p'^j; c_n'^j; c_p''^j; c_n''^j; c_p'''^j$ and $c_n'''^j\}$

Steady-state friction:	$c_p^j = R^j \Delta t \left\| Q_{i-1,t-1}^j \right\|; c_n^j = R^j \Delta t \left\| Q_{i+1,t-1}^j \right\|; R^j = f^j/2D^jA^j$
Unsteady friction:	$c_{p_1}'^j = k_v\theta Q_{i,t-1}^j - k_v(1-\theta)\left(Q_{i-1,t-1}^j - Q_{i-1,t-2}^j\right) - k_v \mathbf{sgn}\left(Q_{i-1,t-1}^j - Q_{i-1,t-1}^j\right)$
	$c_{n_1}'^j = k_v\theta Q_{i,t-1}^j - k_v(1-\theta)\left(Q_{i+1,t-1}^j - Q_{i+1,t-2}^j\right) - k_v \mathbf{sgn}\left(Q_{i+1,t-1}^j - Q_{i+1,t-1}^j\right)$
	$c_{p_2}''^j = c_{n_2}''^j = k_v\theta$; ($\theta = 1$ is a relaxation coefficient)
	$c_{p1}'''^j = -c_{n_1}'''^j = -2a_0^jA^j\Delta t \sum_{k=1}^{n_{kv}} \left[\frac{\varepsilon_{rk}^j(x,t)}{\partial t}\right]$ $\qquad c_{p2}'''^j = c_{n2}'''^j = 2a_0^jA^jc_0\gamma \sum_{k=1}^{n_{kv}} J_k^j(1 - e^{-(\Delta t/\tau_k)})$
Linear-viscoelastic behavior of pipe-wall:	$\varepsilon_{rk,i,t-\Delta t}^j = J_k^jc_0\left\{\left[H_{i,t-\Delta t}^j - H_{i,0}^j\right] - e^{-(\Delta t/\tau_k)}\left[H_{i,t-2\Delta t}^j - H_{i,0}^j\right] - \tau_k'\left(1 - e^{-(\Delta t/\tau_k)}\right)\left[\frac{H_{i,t-\Delta t}^j - H_{i,t-2\Delta t}^j}{\Delta t}\right]\right\} + e^{-(\Delta t/\tau_k)}\varepsilon_{rk,i,t-2\Delta t}$; $c_0 = \frac{a_{0D}^j}{2\theta^j}\gamma$

Cavitating flow modeling

The discrete gas cavity model (DGCM) has been selected in this paper to predict cavitation triggering. This model is described in detail by Wylie & Streeter (1993).

Accordingly, the perfect gas law for the isothermic evolution of each isolated gas cavity may be expressed as follows (Wylie & Streeter 1993; Martins *et al.* 2015):

$$\forall_{gi}^{t}\left(H_i^t - z_i - H_v\right) = (H_0 - z_0 - H_v)\alpha_0 A\Delta x \tag{8}$$

where H_0 and H_v designate the reference and the gauge pressure-head values, respectively; α_0 denotes the void fraction at H_0, and z_i represents the pipe elevation.

As for Wylie & Streeter (1993) and Soares *et al.* (2012), the continuity equation for each isolated gas cavity is discretized as follows:

$$\forall_{gi}^{t} = \forall_{gi}^{t-2\Delta t} + \left[\psi\left(Q_{di}^{t} - Q_{ui}^{t}\right) - (1-\psi)\left(Q_{di}^{t-2\Delta t} - Q_{ui}^{t-2\Delta t}\right)\right]2\Delta t \tag{9}$$

where $\forall_g i$ and $\forall_{gi}^{t-2\Delta t}$ are the discrete cavity volumes at the current time step and at $2\Delta t$ time steps earlier, respectively; Q_u and Q_d designate the flow rates at either side of the cavity zone; and ψ is a weighting factor, chosen in the $0.5 \leq \psi \leq 1$ range (Bergant & Simpson 1999).

It is noteworthy that the incorporation of the DGCM into the numerical model may be based on the cavity volume value criterion: $\forall_{gi,t}^{j} \prec 0$ or $\forall_{gi,t}^{j} \geq 0$, used for distinguishing between one-phase and cavitating flows, respectively.

To achieve the solution at any time step, appropriate boundary conditions should be specified. Specifically, at a junction of a series connection of pipes ($j-1$ and j), the pressure-head and the flowrate may be evaluated using a common hydraulic-grade-line elevation and no flow storage assumptions at this section yields (Wylie & Streeter 1993):

$$H_{|x=L}^{j-1} = H_{|x=0}^{j} \text{ and } Q_{|x=L}^{j-1} = Q_{|x=0}^{j} \tag{10}$$

Model validation

To testify the numerical efficiency of the unconventional water-hammer solver, outlined above, validation is performed using the experimental measurements carried out by Covas *et al.* (2004). The experimental apparatus, considered by the authors, comprises a 271.8 m long HDPE pipe (SDR11/PE100/NP16: nominal diameter: $ND = 63$ mm; wall thickness: $e = 6.25$ mm and internal diameter: $D = 50.6$ mm), a constant level reservoir ($H_0 = 35$ m) located at the upstream end of the pipeline and a ball valve located at the downstream end. A steady-state flow condition, corresponding to a constant flow rate value: $Q_0 = 1.008$ L/s is set up in the hydraulic system prior to the initiation of a transient event provoked by the instantaneous and complete closure of the outlet valve.

The creep compliance coefficients of the generalized Kelvin–Voigt linear viscoelastic mechanical model (five elements), associated to HDPE pipe-wall material creep behavior are $J_{0\cdots5}^{\mathbf{HDPE}} = \{0.069;\ 1.057;\ 1.054;\ 0.905;\ 0.262;\ 0.746\}$ GPa and $\tau_{1\cdots5}^{\mathbf{HDPE}} = \{0.05;\ 0.5;\ 1.5;\ 5.0;\ 10.0\}$ s (Covas *et al.* 2004).

In Figure 3, the numerical results, based on the unconventional water-hammer model using the Vitkovsky unsteady-friction formulations, with and without considering the viscoelastic-behavior of the pipe-wall, are compared against the experimental measurements of Covas *et al.* (2004). Specifically, these pressure heads have been plotted at the downstream valve section.

Figure 3 clearly shows the general agreement between the numerical solution predicted by the unconventional water-hammer model using the Vitkovsky unsteady-friction formulations and the experimental results concerning the amplitude and the phase shift of the first cycle of pressure-head oscillation. Meanwhile, a shift is observed in the subsequent cycles between the experimental and numerical results with regard to the period of pressure wave oscillations.

On the other hand, regarding the numerical results accounting for unsteady friction only, major discrepancies are observed between the experimental and numerical results in terms of amplitude, period and shape of the pressure wave oscillation patterns. Indeed, such a model overestimates the maximum pressure head for the first cycle of wave oscillation.

RESULTS AND DISCUSSION

In the following, the inline strategy, already described, is investigated separately for two test scenarios relating to water-hammer up- and down-surge frameworks.

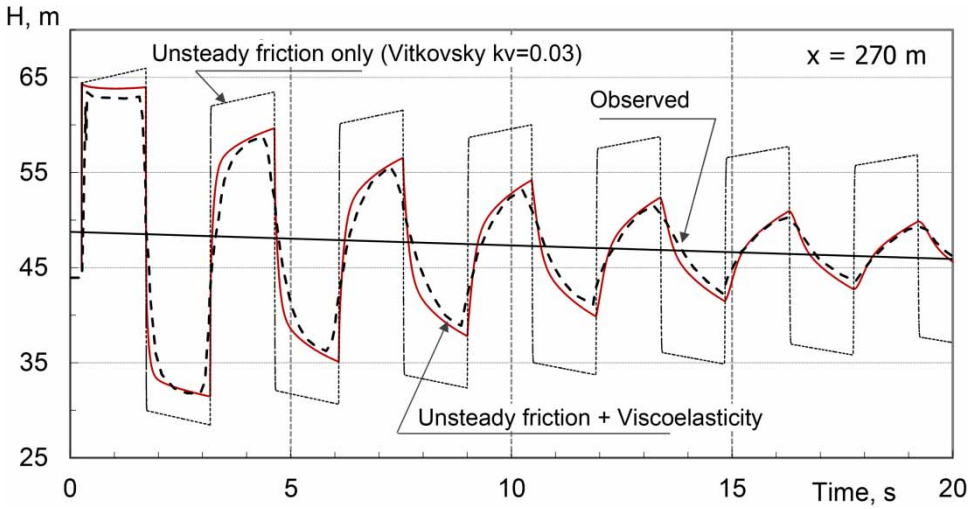

Figure 3 | Comparison of experimental and computed pressure-head evolutions at the downstream valve section.

Furthermore, two types of polymeric material for the pipe-wall of the replaced short-section are employed in each scenario, comprising HDPE and LDPE pipe-wall material: $J_{0\cdots5}^{\mathbf{HDPE}} = \{0.069;\ 1.057;\ 1.054;\ 0.905;\ 0.262;\ 0.746\}$ GPa; $\tau_{1\cdots5}^{\mathbf{HDPE}} = \{0.05;\ 0.5;\ 1.5;\ 5.0;\ 10.0\}$ s (Covas *et al.* 2004, 2005) and LDPE material: $J_{0\cdots3}^{\mathbf{LDPE}} = \{1.54;\ 7.54;\ 10.46;\ 12.37\}GPa$; $\tau_{1\cdots3}^{\mathbf{LDPE}} = \{0.000089;\ 0.022;\ 1.864\}s$ (Güney 1983).

As regards the following numerical results, calculations were carried out using the FG-MOC algorithm outlined above.

Investigation of water-hammer up-surge control

This subsection is devoted to applying the proposed water-hammer control strategy within the up-surge framework. The hydraulic system, considered herein, is composed of the reservoir-pipe-valve system illustrated in Figure 4(a). The main steel pipeline specifications are: $E_0^{\mathbf{Steel}} = 206$ GPa; $L = 143.7$ m; $D = 50.6$ mm; $e = 3.35$ mm and $a_0^{\mathbf{Steel}} = 1372.78$m/s. The initial steady-state flow conditions are described by a constant flow rate: $Q_0 = 0.58$ L/s and a constant pressure head: $H_{0R} = 45$ m, maintained at the

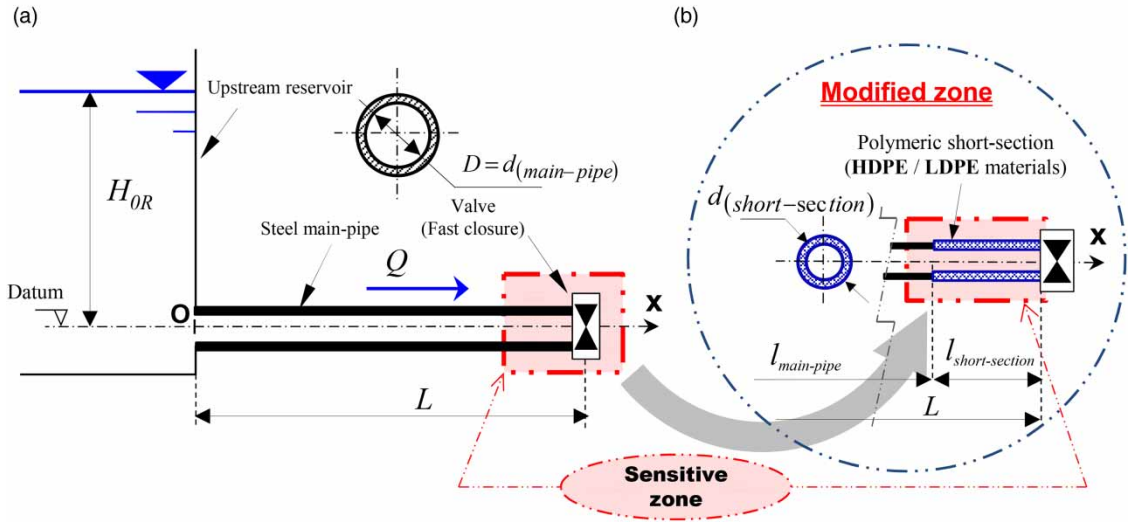

Figure 4 | Schematic setups of: (a) primitive (non-controlled) system; (b) controlled system using the inline-strategy, for the up-surge control test-case.

upstream reservoir. The water-hammer up-surge is initiated by an instantaneous and full switch-off of the downstream valve. The boundary conditions relative to such a water-hammer event may be expressed as follows:

$$Q_{|x=L} = 0 \text{ and } H_{|x=0} = H_{0R} \ (t \succ 0) \tag{11}$$

For instance, since the transient event is initiated at the downstream end of the piping system, the control strategy would consist of replacing a downstream short-section of the main steel-piping system by another made of a polymeric pipe-wall material (Figure 4(b)). The short-section length and diameter are: $l_{short-section} = 5$ m and $d_{short-section} = 50.6$ mm, respectively. Incidentally, it is important to note that the length of the modified steel-piping system is reduced (from its original value: $L = 143.7$ m) to: $l_{main-pipe} = L - l_{short-section} = 138.7$ m.

One notes that the subsequent numerical computations were carried out using an FG-MOC algorithm, with a specified time step $\Delta t = 0.018$ s resulting in Courant numbers of $C^r_{main-pipe} = 0.9709$ and $C^r_{short-section} = 1$, corresponding to the steel main-pipe and the polymeric short-section discretization.

Estimation results of the pressure-head, total circumferential-stress and retarded radial-strains, evaluated at the downstream valve section ($x = L$), versus time, predicted into the unprotected system, along with the corresponding profiles computed for the protected system employing an HDPE or an LDPE short-section, are graphed in Figure 5(a)–5(c), respectively.

Clearly, Figure 5(a) illustrates the attenuation effects of the first pressure-head peak along with a period spread-out of wave oscillations for the protected system cases. Particularly, the up-surge magnitude values observed in the protected systems using HDPE or LDPE short-section materials are: $H_{\max}^{(\text{Steel}+\text{HDPE})\ \text{pipe}} = 77.92$ m and $H_{\max}^{(\text{Steel}+\text{LDPE})\ \text{pipe}} = 65.31$ m, respectively, which are relatively lower than the corresponding magnitude value observed in the original unprotected system ($H_{\max}^{\text{Steel pipe}} = 85.59$ m). In return, the up-surge attenuations performed by the employed control strategy using HDPE and LDPE short-section materials are: $\Delta H_{up-surge}^{\text{HDPE}} = H_{\max}^{\text{Steel pipe}} - H_{\max}^{(\text{Steel}+\text{HDPE})\ \text{pipe}} = 7.67$ m and $\Delta H_{up-surge}^{\text{LDPE}} = H_{\max}^{\text{Steel pipe}} - H_{\max}^{(\text{Steel}+\text{LDPE})\text{pipe}} = 20.28$ m, respectively. Furthermore, the amortization rate of the first pressure-head peak is slightly more important for the case using an LDPE short-section ($\mu^{\text{LDPE}} = \{H_{\max}^{(\text{Steel}+\text{LDPE})\ \text{pipe}} - H_{\max}^{\text{Steel pipe}}\}/\Delta H_{up-surge}^{\text{Steel pipe}} = 49.96\,\%$) than the one obtained using an HDPE short-section ($\mu^{\text{HDPE}} = 18.89\,\%$).

Similarly, Figure 5(b) illustrates that the employed technique could also significantly lessen the first circumferential-stress peak compared with the one predicted into the unprotected system. More precisely, these attenuations are more important for the case using an LDPE short-section (i.e.: $\Delta\sigma_{up-surge}^{\text{LDPE}} = \sigma_{\max}^{\text{Steel pipe}} - \sigma_{\max}^{(\text{Steel}+\text{LDPE})\ \text{pipe}} = 1.94$ MPa) than those obtained using an HDPE short-section (i.e.: $\Delta\sigma_{up-surge}^{\text{HDPE}} = \sigma_{\max}^{\text{Steel pipe}} - \sigma_{\max}^{(\text{Steel}+\text{HDPE})\ \text{pipe}} = 0.31$ MPa).

Contrary to the pressure-head and circumferential-stress charts interpreted above, Figure 6(c) displays an amplification of the retarded radial-strain peaks. Particularly, for the case using an HDPE short-section, the magnitude of the first retarded radial-strain peak is $\Delta\varepsilon_{up-surge}^{(\text{Steel}+\text{HDPE})\ \text{pipe}} = 4.64$ mm/m. Furthermore, a more amplified amplitude is depicted for the case using an LDPE short-section, corresponding to: $\Delta\varepsilon_{up-surge}^{(\text{Steel}+\text{LDPE})\ \text{pipe}} = 8.94$ mm/m, while the corresponding amplitude is equal to $\Delta\varepsilon_{up-surge}^{\text{Steel pipe}} = 26\ \mu$m/m, for the unprotected system case. Incidentally, this result was physically expected based on the viscoelastic behavior of polymeric pipe-wall material which has a retarded radial-strain component, in addition to the elastic radial strain observed in an elastic pipe-wall material, such as steel.

As a further examination of the wave patterns plotted in Figure 6(a)–6(c), it is worth noting that the employed control strategy induces a period spread-out of the first cycle of wave oscillations compared with the unprotected original hydraulic system. Precisely, the period of wave oscillations computed into the protected system employing an HDPE or LDPE short-section are: $T_{1^{st}Cycle}^{(\text{Steel}+\text{HDPE})\ \text{pipe}} = 0.8$ s or $T_{1^{st}Cycle}^{(\text{Steel}+\text{LDPE})\ \text{pipe}} = 1.24$ s, respectively, whereas the corresponding period, predicted into the original unprotected system is equal to $T_{1^{st}Cycle}^{\text{Steel pipe}} = 0.4$ s. Consequently, the implementation of the inline control strategy (i.e. the use of inline polymeric pipe-wall short-sections) produces the spread-out of the period of pressure-head, circumferential-stress and radial-strain oscillations.

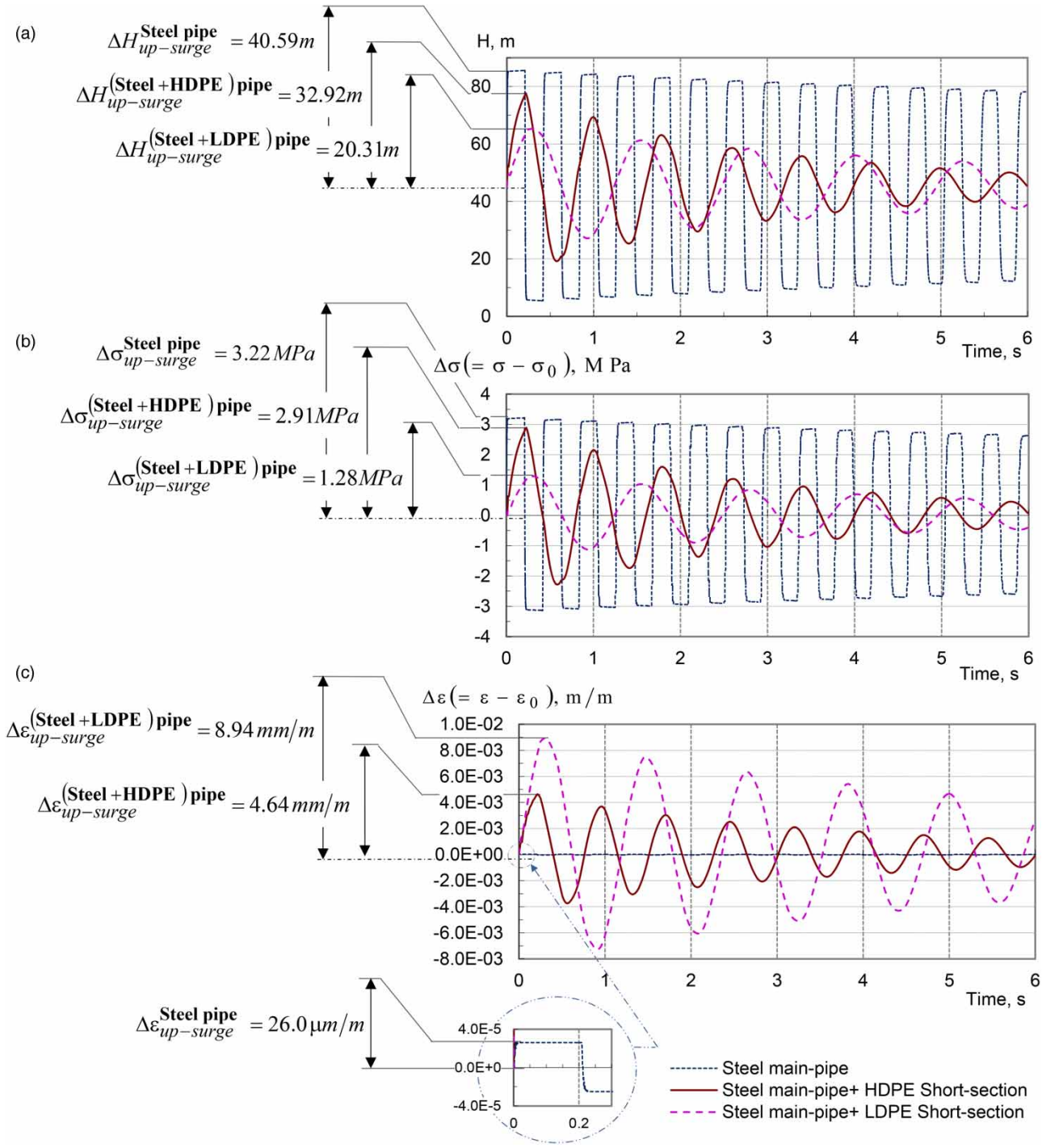

Figure 5 | Comparison of (a) pressure-head, (b) circumferential-stress and (c) radial-strain, versus time, at the downstream valve section for the primitive and the inline strategy based controlled hydraulic systems.

Once the main key features of the inline control strategy were addressed for specific short-section diameter and length values, it would be interesting to explore the magnitude sensitivity of the first maximum pressure-head, stress and total-strain peaks according to the foregoing parameters. For completeness, these peak traces, evaluated at

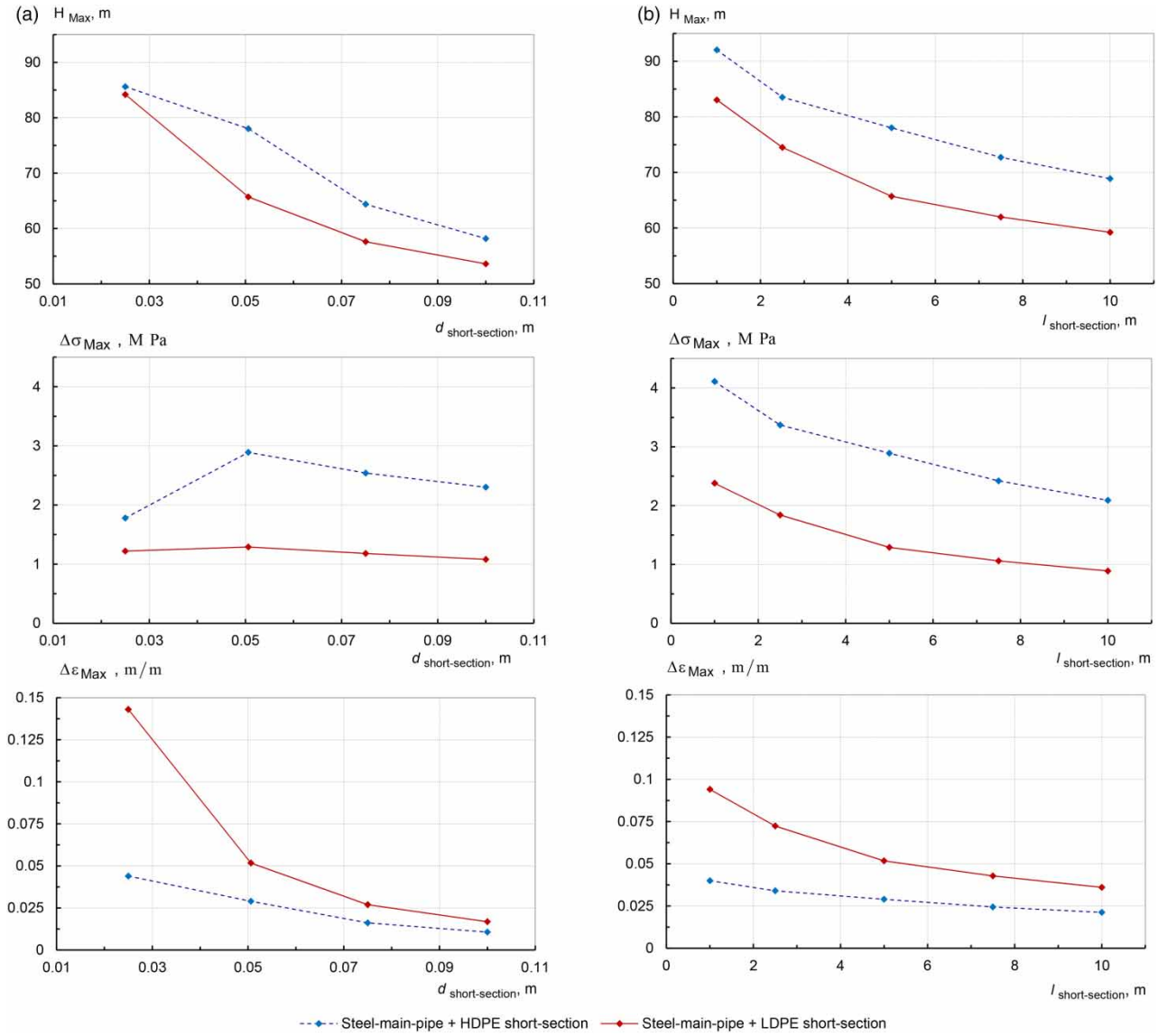

Figure 6 | Variation of downstream pressure-heads, circumferential-stress and radial-strain peaks depending on the short-section: (a) diameter (for $d_{\text{short-section}} = 50.6$ mm) and (b) length (for $l_{\text{short-section}} = 5$ m).

the downstream pipe section, in terms of short-section diameter and length, are illustrated in Figure 6(a) and 6(b), respectively. In particular, the following parameter sets are presented: $d_{short-section} = \{0.025;\ 0.0506;\ 0.075 \text{ and } 0.1 \text{ m}\}$ and $l_{short-section} = \{1;\ 2.5;\ 7.5;\ \text{and } 10 \text{ m}\}$.

As expected, the general trend of these graphs revealed that the magnitude of the first maximum peaks of pressure head and circumferential stress decreased (and inversely, the first maximum radial-strain peak increased) as the short-section size increased. For example, Figure 6(a) clearly illustrates that as the short-section diameter increased, the magnitude of the first maximum peaks of pressure head and circumferential stress decreased (and inversely, the first maximum radial-strain peak increase). However, the foregoing effect is markedly higher for the diameter values below: $d_{short-section} \leq 0.075$ m than those for the rest of the diameter range. The same trend is observed for the length values below: $l_{short-section} \leq 5$ m (Figure 6(b)). Accordingly, the diameter and length values: $\{d_{short-section} = 0.075 \text{ m and } l_{short-section} = 5 \text{ m}\}$ may be selected as being a near-optimal value for the short-section size.

The first investigations have outlined that the inline control strategy can successively be employed to dampen water-hammer up-surge waves. Furthermore, the robustness of this strategy with regard to water-hammer down-surge framework is checked in the following subsection.

Investigation of water-hammer down-surge control

The hydraulic system considered in this subsection is shown in Figure 7(a). The apparatus consists of a sloping steel pipeline ($L = 100\,\text{m}; d = 44.1\,\text{mm}$; $E_0^{\text{Steel}} = 210\,\text{GPa}$ and $a_0^{\text{Steel}} = 1302.512\,\text{m/s}$) connecting two pressurized tanks and equipped with a ball valve at its inlet. The downstream pipe axis is taken as the horizontal datum level ($z_d = 0\,\text{m}$), and the upstream tank level is $z_u = 2.03\,\text{m}$. The gauge pressure head of the liquid is $H_g = -10.29\,\text{m}$. A steady-state flow condition, corresponding to a velocity $V_0 = 1.04\,\text{m/s}$ and a constant pressure-head $H_0^{T_2} = 21.4\,\text{m}$ maintained at the downstream pressurized tank, are set up in the hydraulic system prior to the initiation of a transient event produced by the instantaneous switch-off of the downstream valve. For this particular flow scenario, the boundary conditions may be expressed as follows:

$$Q_{|x=0} = 0 \text{ and } H_{|x=L} = H_0^{T_2} \ (t \succ 0) \tag{12}$$

For instance, since the transient event is induced at the upstream extremity, the piping system is handled at this extremity through the replacement of an upstream short-section of the main steel-pipe by another one made of polymeric pipe-wall material. Thereby, the hydraulic system may be modified as schematically illustrated in Figure 7(b). The short-section length and diameter values are $l_{short-section} = 10\,\text{m}$ and $d_{short-section} = 44.1\,\text{mm}$, respectively.

One notes that further water-hammer calculations are achieved using an FG-MOC algorithm, in conjunction with the DGCM. The time step was set to: $\Delta t = 0.034\,\text{s}$, resulting

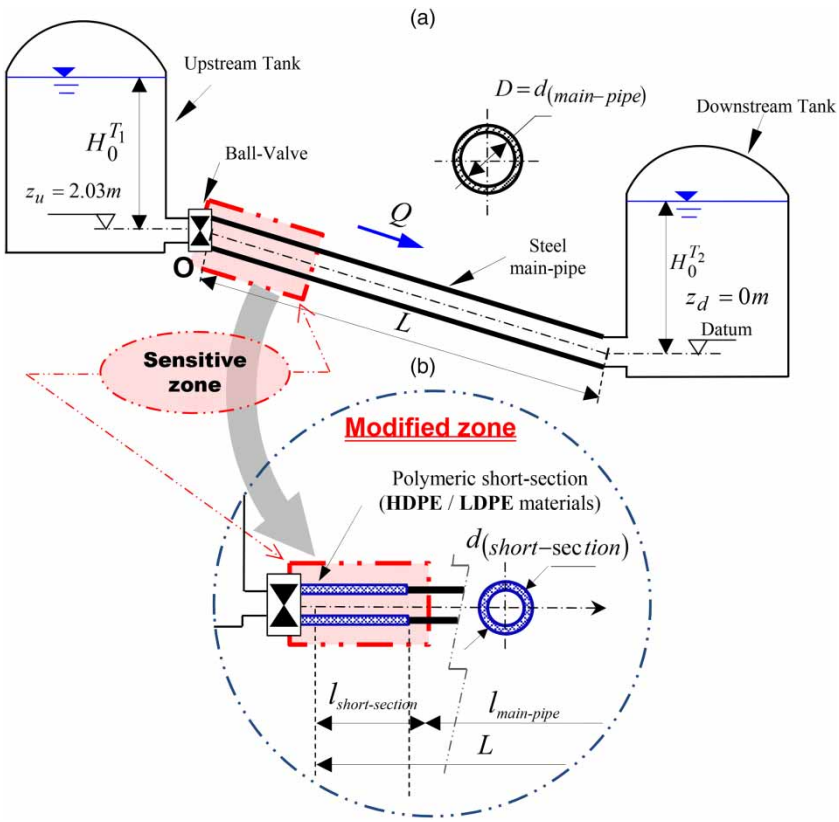

Figure 7 | Schematic setups of: (a) primitive (non-controlled) system; (b) controlled system using the inline-strategy, for the down-surge control test-case.

in Courant numbers of: $C^r_{main-pipe} = 0.948$ and $C^r_{short-section} = 1$ associated with the steel-pipe and the polymeric short-section discretization, and a weighting factor $\psi = 0.5$.

Figure 7(a)–7(c) consider the upstream pressure-head, total circumferential-stress and retarded radial-strains traces, versus time, computed for the unprotected hydraulic systems, along with the corresponding profiles predicted into the protected system employing HDPE and LDPE short-sections.

Clearly, Figure 7(a) illustrates an impulse wave pattern of the flow behavior predicted into the unprotected hydraulic system. Incidentally, the generation of these impulse waves is closely associated with the upstream valve switch-off. Specifically, for the unprotected system case, Figure 8(a) reveals that the pressure head firstly drops below the saturated pressure-head value of the liquid ($H^{\textbf{Steel pipe}}_{\min} = -10.2$ m) and, subsequently, rises to $H^{\textbf{Steel pipe}}_{\max} = 63.7$ m, which corresponds to the of the up- and down-surge magnitude values $\Delta H^{\textbf{Steel pipe}}_{down-surge} = 31.69$ m and $\Delta H^{\textbf{Steel pipe}}_{up-surge} = 42.3$ m, respectively, above the initial steady state value.

Alternatively, Figure 8(a) indicates that the cavitating flow onset may be avoided if the proposed control strategy is employed. Particularly, analysis of the pressure-head curves, computed for the corresponding transient event induced into the protected hydraulic system, displays low magnitude values compared with the unprotected case discussed above. Particularly, the proposed control strategy allows pressure-head drop attenuations $\Delta H^{\textbf{HDPE}}_{down-surge} = H^{(\textbf{Steel + HDPE}) \textbf{ pipe}}_{\min} - H^{\textbf{Steel pipe}}_{\min} = 7.16$ m or $\Delta H^{\textbf{LDPE}}_{down-surge} = H^{(\textbf{Steel + LDPE}) \textbf{ pipe}}_{\min} - H^{\textbf{Steel pipe}}_{\min} = 11.61$ m for the case utilizing an HDPE or LDPE short-section. Furthermore, it is important to delineate that the LDPE short-section pipe-wall material provides more amortization of pressure-head drop than the HDPE one. Precisely, the down-surge amortization rates obtained utilizing an HDPE or LDPE short-section are: $\mu'^{\textbf{HDPE}} = \{H^{(\textbf{Steel + LDPE}) \textbf{ pipe}}_{\min} - H^{\textbf{Steel pipe}}_{\min}\}/\Delta H^{\textbf{Steel pipe}}_{down-surge} = 22.62\,\%$ or $\mu'^{\textbf{LDPE}} = 47.35\%$, respectively.

A further observation from Figure 8(a) relates to the ability of the proposed strategy to also allow a significant damping of the first up-surge peak. Specifically, the damping of the maximum pressure head observed for the case using HDPE or LDPE polymeric materials of the short section are: $\Delta H^{\textbf{HDPE}}_{up-surge} = H^{\textbf{Steel pipe}}_{\max} - H^{(\textbf{Steel + HDPE}) \textbf{ pipe}}_{\max} = 20.76$ m and $\Delta H^{\textbf{LDPE}}_{up-surge} = H^{\textbf{Steel pipe}}_{\max} - H^{(\textbf{Steel + LDPE}) \textbf{ pipe}}_{\max} = 30.39$ m, respectively. In return, the employed strategy provides an amortization rate of the first maximum pressure-head peak equal to $\mu^{\textbf{LDPE}} = 71.84\%$ or $\mu^{\textbf{HDPE}} = 49.09\%$ for the cases utilizing LDPE or HDPE short-sections.

Additional observations concerning the upstream circumferential-stress and radial-strain patterns plotted on Figure 8(b) and 8(c), respectively, may be analyzed with analogy to the foregoing up-surge control test case. Particularly, Figure 8(b) shows that the magnitude of the first circumferential-stress ridge is equal to $\Delta\sigma^{(\textbf{Steel + HDPE}) \textbf{ pipe}}_{down-surge} = 1.93$ MPa for the case using an HDPE short-section. Likewise, a much lower value of the first circumferential-stress ridge magnitude is observed for the case made of LDPE short-section: $\Delta\sigma^{(\textbf{Steel + LDPE}) \textbf{ pipe}}_{down-surge} = 0.665$ MPa, while the corresponding value is equal to $\Delta\sigma^{\textbf{Steel pipe}}_{down-surge} = 3.52$ MPa for the unprotected system case.

Nonetheless, regarding the upstream radial-strain pattern of Figure 8(c), these curves indicate a limitation of the inline strategy arising from the excessive amplification of radial strain observed within the controlled system frames. As previously mentioned, this is due to the utilization of the high-deformable material for the replaced short-section pipe-wall. Specifically, the magnitude of the first radial-strain ridge is $\Delta\varepsilon^{(\textbf{Steel + HDPE}) \textbf{ pipe}}_{down-surge} = 2.127$ mm/m, for the case using an HDPE short-section. Likewise, a more important magnitude value is observed for the case using an LDPE short-section corresponding to: $\Delta\varepsilon^{(\textbf{Steel + LDPE}) \textbf{ pipe}}_{down-surge} = 3.996$ mm/m. $\Delta\sigma^{(\textbf{Steel + LDPE}) \textbf{ pipe}}_{down-surge} = 0.665$ MPa, whereas the corresponding value is equal to $\Delta\varepsilon^{\textbf{Steel pipe}}_{down-surge} = 10.7 \times 10^{-3}$ mm/m for the unprotected system case.

As for the up-surge control test case, the analysis second step will target the dependence of the magnitude of the first pressure head, circumferential stress and radial-strain ridge on the short-section diameter and length parameters. For completeness, the results of latter behavior are addressed in Figure 9(a) and 9(b), respectively for the diameter and length value sets: $d_{short-section} = \{0.045;\ 0.0506; 0.075$ and 0.1 m$\}$ and $l_{short-section} = \{5;\ 7.5;\ 10;\ 12.5$ and 15 m$\}$.

These curves indicate that, as far as the inline short-section diameter or length increases, the value of the minimum ridges of transient pressure head, circumferential stress (and

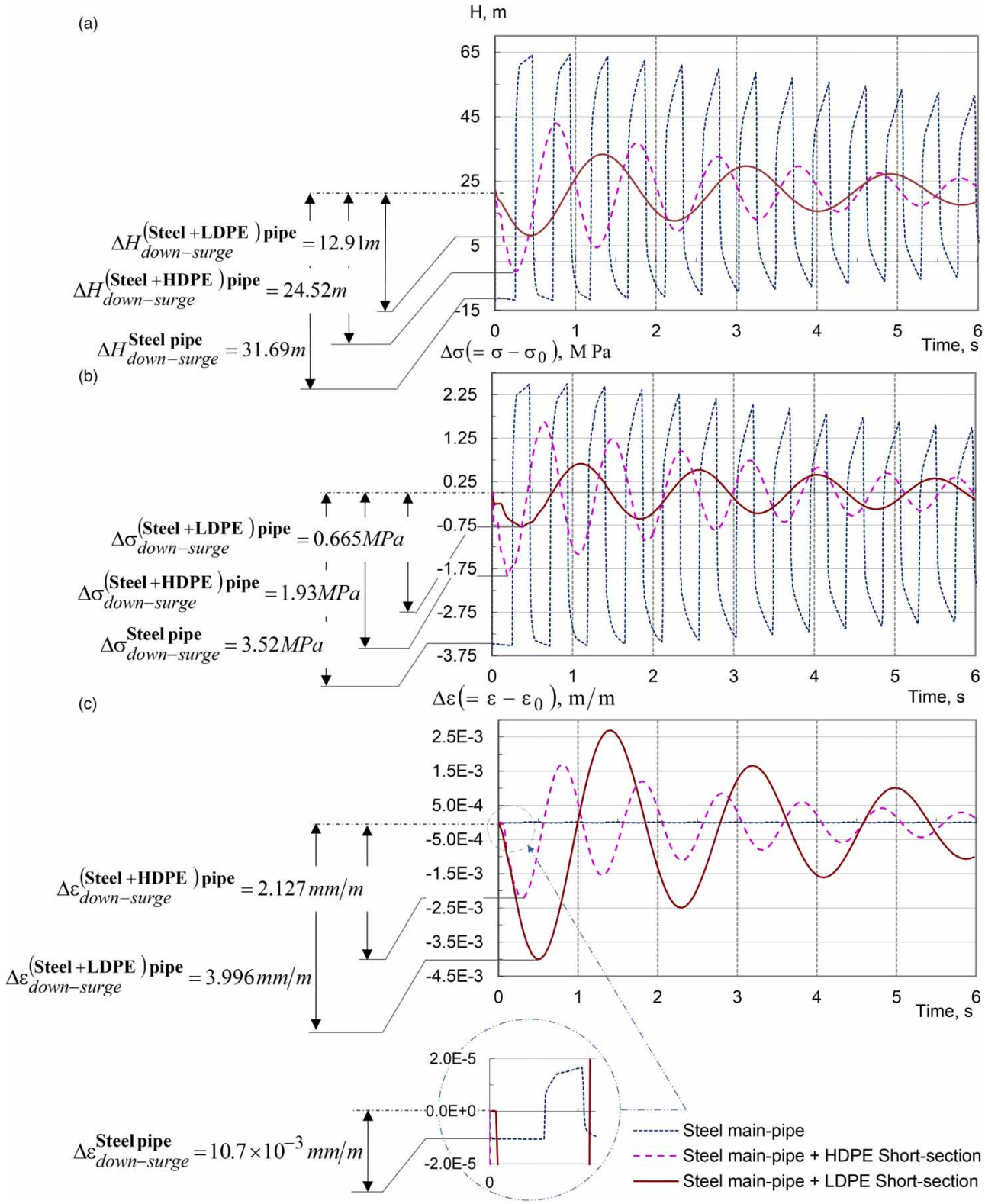

Figure 8 | Comparison of (a) pressure-head, (b) circumferential-stress and (c) radial-strain, versus time, at the upstream valve section for the primitive and the inline strategy based controlled hydraulic systems.

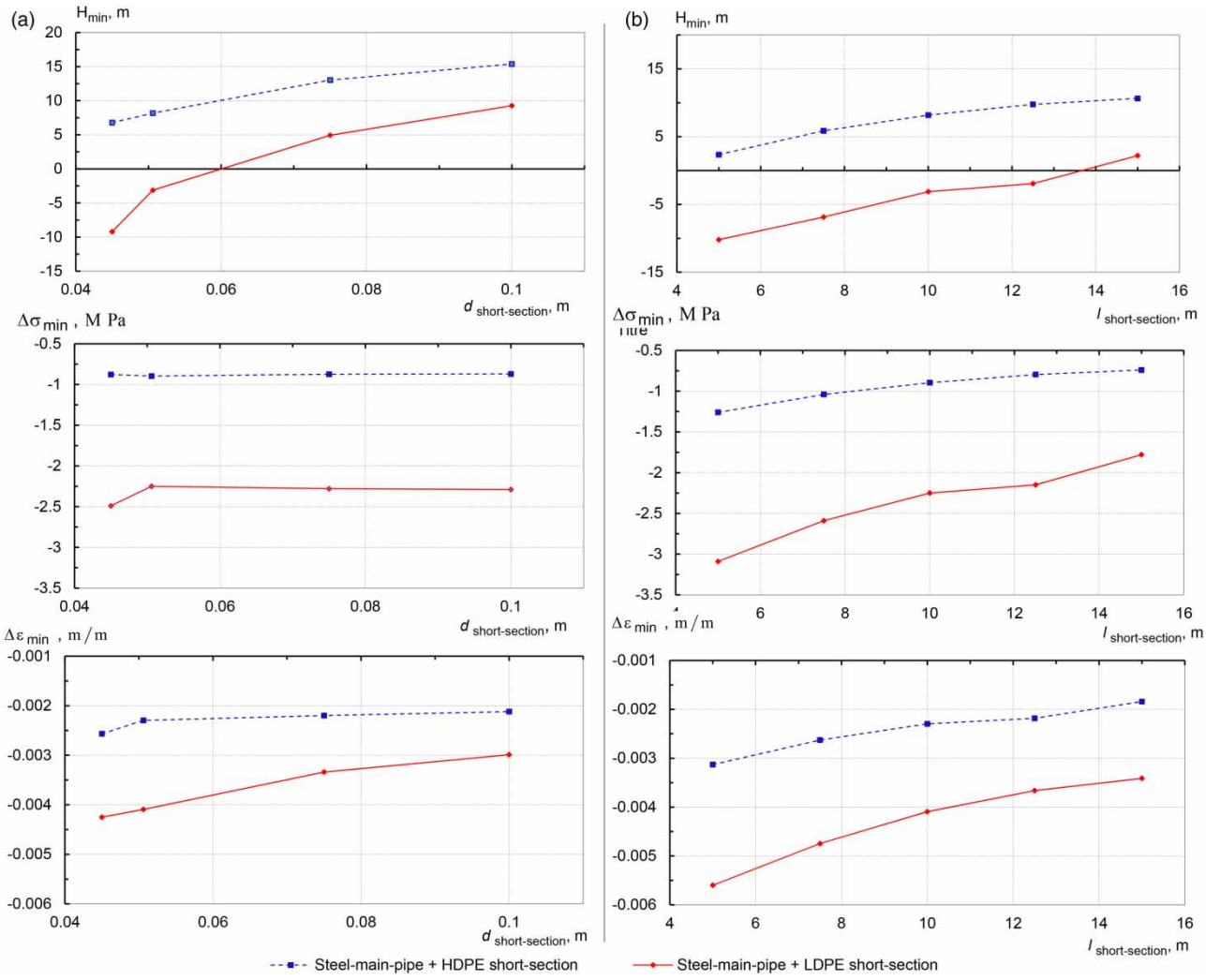

Figure 9 | Variation of upstream pressure-heads, circumferential-stress and radial-strain ridges depending on the short-section: (a) diameter (for $d_{\text{short-section}} = 50.6$ mm) and (b) length (for $l_{\text{short-section}} = 10$ m).

radial-strain) decreases. However, these effects are much less visible for the diameter and length values: $d_{short-section} \geq 0.075$ m and $l_{short-section} \geq 10$ m, respectively. Thus, for the case studied herein, the diameter and length values: $\{d_{short-section} = 0.075 \text{ m} \quad \text{and} \quad l_{short-section} = 10 \text{ m}\}$ may be selected as an optimal estimation of the short-section size.

CONCLUSIONS

Overall, it is estimated that the present study emphasized the importance of characterizing additional design parameters, such as the circumferential-stress and the radial-strain parameters in supplement of the pressure-head one. Moreover, the unconventional water-hammer model, based on the Kelvin–Voigt and the Vitkovsky formulations, is regarded as a valuable numerical tool to provide comprehensive information on physical parameters required by designers.

Furthermore, the present study has highlighted that the use of inline based water-hammer control re-design strategy has the potential to mitigate severe water-hammer courses. Computational examples illustrate a large amortization of the first pressure head and circumferential-stress rise (and drop) associated with both up- and down-surge scenarios. Furthermore, it is important to delineate that the use of

LDPE material for the short-section pipe-wall allows significant amortizations compared with the corresponding case utilizing HDPE material.

However, it should be emphasized that such a control strategy produces an amplification of the radial strain throughout the employed polymeric short-section, along with a delay of a subsequent steady-state regime. This insight can possibly unveil additional design criteria. Such criteria can limit the performance of the proposed strategy.

Additionally, the sensitivity analysis of the pressure-head, circumferential-stress and radial-strain peak (and ridge) magnitudes with regard to the short-section length and diameter provided an estimation of optimal cost-effectiveness values for these parameters.

It is estimated that the results obtained in the present study can provide some physical insights into the water supply design side to mitigate the severe effects of water-hammer surges, besides providing the adequate service level of these utilities. A more general framework, such as water supply networks, is worth further investigation.

REFERENCES

Aklonis, J. J., MacKnight, W. J. & Shen, M. 1972 *Introduction to Polymer Viscoelasticity.* Wiley-Interscience, John Wiley & Sons, Inc., New York.

Bergant, A. & Simpson, A. 1999 Pipeline column separation flow regimes. *J. Hydraul. Eng. ASCE* **125**, 835–848.

Bergant, A., Simpson, A. R. & Tijsseling, A. 2006 Waterhammer with column separation: a historical review. *J. Fluids Struct.* **22** (2), 135–171.

Boulos, P. F., Karney, B. W., Wood, D. J. & Lingireddy, S. 2005a Pressure vessels and piping systems – shock and waterhammer loading. *Am. Water Works Assoc.* **97** (5), 111–124.

Boulos, P. F., Karney, B. W., Wood, D. J. & Lingireddy, S. 2005b Hydraulic transient guidelines for protecting water distribution systems. *Am. Water Works Assoc.* **97** (5), 111–124.

Brinson, H. F. & Brinson, L. C. 2008 *Polymer Engineering Science and Viscoelasticity: an Introduction.* Springer, New York.

Covas, D., Stoianov, I., Ramos, H., Graham, N., Maksimovic, C. & Butler, D. 2004 Waterhammer in pressurized polyethylene pipes: conceptual model and experimental analysis. *Urban Water J.* **1** (2), 177–197.

Covas, D., Stoianov, I., Mano, J. F., Ramos, H., Graham, N. & Maksimovic, C. 2005 The dynamic effect of pipe-wall viscoelasticity in hydraulic transients. Part II-model development, calibration and verification. *J. Hydraul. Res.* **43** (1), 56–70.

Evangelista, S., Leopardi, A., Pignatelli, R. & de Marinis, G. 2015 Hydraulic transients in viscoelastic branched pipelines. *J. Hydraul. Eng.* **141** (8), 04015016.

Ghidaoui, M. & Karney, B. 1994 Equivalent differential equations in fixed-grid characteristics method. *J. Hydraul. Eng.* **120** (10), 1159–1175.

Ghidaoui, M. S., Zhao, M., Duncan, A. M. & David, H. A. 2005 A review of waterhammer theory and practice. *Appl. Mech. Rev.* **58**, 49–76.

Güney, M. S. 1983 Waterhammer in viscoelastic pipes where cross-section parameters are time dependent. In: *Proc. 4th Int. Conf. on Pressure Surges*, BHRA, Bath, UK, pp. 189–209.

Kaveh, H. A., Faig, B. O. N. & Akbar, K. H. 2010 Some aspects of physical and numerical modeling of waterhammer in pipelines. *Nonlinear Dyn.* **60**, 677–701.

Martins, S., Ramos, H. & Almeida, A. 2015 Conceptual analogy for modelling entrapped air action in hydraulic systems. *J. Hydraul. Res.* **53** (5), 678–686.

Massouh, F. & Comolet, R. 1984 Étude d'un système anti-bélier en ligne (Study of a waterhammer protection system in line). *Houille Blanche* **5**, 355–362.

Niroomandi, A., Borghei, S. M. & Bohluly, A. 2012 Implementation of time splitting projection method in water hammer modeling in deformable pipes. *Int. J. Press. Vessels Piping* **98**, 30–42.

Pejovic, S., Boldy, A. P. & Obradovic, D. 1987 *Guidelines to Hydraulic Transient Analysis.* Technical Press, Brookfield, VT.

Pothof, I. & Karney, B. 2012 Guidelines for transient analysis in water transmission and distribution systems. In: *IWA Water Loss Conf.*, International Water Association (IWA), London, pp. 1–12.

Ramos, H., Covas, D., Borga, A. & Loureiro, D. 2004 Surge damping analysis in pipe systems: modelling and experiments. *J. Hydraul. Res.* **42** (4), 413–425.

Seog, J. B. & Karney, B. 2004 Fluid transients and pipeline optimization using GA and PSO: the diameter connection. *Urban Water J.* **1** (2), 167–176 doi:10.1080/15730620412331289995.

Soares, A., Covas, D. & Reis, L. 2008 Analysis of PVC pipe-wall viscoelasticity during waterhammer. *J. Hydraul. Eng.* **134** (9), 1389–1394.

Soares, A., Covas, D. & Carriço, N. 2012 Transient vaporous cavitation in viscoelastic pipes. *J. Hydraul. Res.* **50** (2), 228–235.

Triki, A. 2016 Waterhammer control in pressurized-pipe flow using an in-line polymeric short-section. *Acta Mech.* **227** (3), 777–793.

Triki, A. 2017 Water-hammer control in pressurized-pipe flow using a branched polymeric penstock. *J. Pipeline Syst. Eng. Pract. ASCE* **8** (4), 04017024.

Vitkovsky, J. P., Lambert, M. F., Simpson, A. R. & Bergant, A. 2000 Advances in unsteady friction modelling in transient pipe flow. In: *Eighth International Conference on Pressure Surges*, BHR, The Hague, The Netherlands.

Wylie, E. B. & Streeter, V. L. 1993 *Fluid Transients in Systems.* Prentice Hall, Englewood Cliffs, NJ.

First received 11 July 2016; accepted in revised form 27 July 2017. Available online 27 September 2017